

# Ocean–atmosphere processes driving Indian summer monsoon biases in CFSv2 hindcasts

Balachandrudu Narapusetty<sup>1,2</sup> · Raghu Murtugudde<sup>1</sup> · Hui Wang<sup>3</sup> · Arun Kumar<sup>4</sup>

Received: 24 April 2015 / Accepted: 30 October 2015 / Published online: 15 December 2015  
© The Author(s) 2015. This article is published with open access at Springerlink.com

**Abstract** This paper analyzes the role of the Indian Ocean (IO) and the atmosphere biases in generating and sustaining large-scale precipitation biases over Central India (CI) during the Indian summer monsoon (ISM) in the climate forecast system version 2 (CFSv2) hindcasts that are produced by initializing the system each month from January 1982 to March 2011. The CFSv2 hindcasts are characterized by a systematic dry monsoon bias over CI that deteriorate with forecast lead-times and coexist with a wet bias in the tropical IO suggesting a large-scale interplay between coupled ocean–atmosphere and land biases. The biases evolving from spring-initialized forecasts are analyzed in detail to understand the evolution of summer biases. The northward migration of the Inter Tropical Convergence Zone (ITCZ) that typically crosses the equator in the IO sector during April in nature is delayed in the hindcasts when the forecast system is initialized in early spring. Our analyses show that the delay in the ITCZ coexists with wind and SST biases and the associated processes project onto the seasonal evolution of the coupled ocean–atmosphere features. This delay in conjunction with the SST and the wind biases during late spring and early summer contributes to excessive precipitation over the ocean and leading to a deficit in rainfall over CI throughout the summer. Attribution of

bias to a specific component in a coupled forecast system is particularly challenging as seemingly independent biases from one component affect the other components or are affected by their feedbacks. In the spring-initialized forecasts, the buildup of deeper thermocline in association with warmer SSTs due to the enhanced Ekman pumping in the southwest IO inhibits the otherwise typical northward propagation of ITCZ in the month of April. Beyond this deficiency in the forecasts, two key ocean–atmosphere coupled mechanisms are identified; one in the Arabian Sea, where a positive windstress curl bias in conjunction with warmer SSTs lead to a weakening of Findlater jet and the other in the east equatorial IO where a remote forcing by the predominantly westerly bias in the western-central equatorial IO in the summer strengthen the seasonal downwelling Kelvin wave that in turn deepens the thermocline in the eastern IO. The equatorial Kelvin wave continues as a coastal Kelvin wave and disperses as Rossby waves off Sumatra and induces positive SST and precipitation biases in the eastern and southern Bay of Bengal. This study shows that the biases that first appear in winds lead to a cascade of coupled processes that exacerbate the subsequent biases by modulating the evolution of seasonal processes such as the annual Kelvin and Rossby waves and the cross-equatorial vertically integrated moisture transport. While this analysis does not offer any particular insights into improving the ISM forecasts, it is a foundational first step towards this goal.

✉ Balachandrudu Narapusetty  
bnarapus@umd.edu

<sup>1</sup> Earth System Science Interdisciplinary Center, University of Maryland, College Park, MD, USA

<sup>2</sup> Hydrological Sciences Laboratory, NASA Goddard Space Flight Center, Greenbelt, MD, USA

<sup>3</sup> INNOVIM and NOAA/NCEP/Climate Prediction Center, College Park, MD, USA

<sup>4</sup> NOAA/NWS/NCEP/Climate Prediction Center, College Park, MD, USA

**Keywords** CFSv2 forecast biases · Indian summer monsoon rainfall · Dry-land biases

## 1 Introduction

A skillful forecast of the Indian summer monsoon rainfall (ISMRF) is pivotal to the economy, agriculture and

water-resources for more than a billion people. ISMR forecasts have been issued based on statistical modeling techniques for several decades with limited success (Rajeevan 2001; Gadgil et al. 2005) but dynamic forecasting efforts are now becoming routine (Borah et al. 2013; Abhilash et al. 2014). The seasonal evolution of monsoonal rainfall is sensitive to the coupled ocean–atmosphere processes in the Indian Ocean (IO), and the Arabian Sea (AS) among the others. SST variations in the IO and the AS could have a profound influence on atmospheric circulation that significantly affects the ISMR by limiting moisture availability or weakening the atmospheric circulation such as Findlater jet (Shukla 1975; Vecchi and Harrison 2004; Vecchi et al. 2004; Levine and Turner 2012; Sayantani et al. 2014). The SSTs in the AS and IO are remotely affected by each other through atmospheric processes; for instance, the warmer SSTs in the Seychelles–Chagos thermocline ridge induce changes in the low-level atmospheric circulation that causes weaker upwelling in the AS and eventually leads to increased precipitation along the Western Ghats (Murtugudde et al. 1998; Izumo et al. 2008).

The current advances in state-of-the-art dynamical modeling approaches blended with data assimilation techniques equip the coupled general circulation models (CGCMs) to skillfully forecast key global features such as El Niño–Southern Oscillation (ENSO) and thus provide a dynamical framework to forecast ISMR. However, the skillful ISMR forecasting is still a challenging task due to the fact that the prediction skill depends, among the other things, on the interactions among the ocean, atmosphere and land components of the CGCMs, which are not captured accurately by the models. On the positive side, current CGCM forecast systems show some prediction skill in reproducing the ISMR when they are initialized in late spring (DelSole and Shukla 2012). The CGCM forecast systems are known to exhibit systematic biases in capturing the seasonal features of the global circulation and the process-based understanding of the evolution of biases involving interactions among the system components should lead to an improved understanding for their causes. Lee et al. (2010) examined the biases in a suite of coupled forecast systems and found that the seasonal prediction skill is positively correlated with the ability to reproduce the mean-state and the annual cycle. We extend this approach by focusing on the evolution of the biases leading up to the target of the analysis, i.e., the dry continental bias in the ISM in CFSv2 hindcasts.

A posteriori bias correction by subtracting the systematic biases, especially involving SSTs, is a common practice to correct the model drift in CGCM decadal forecasts and climate change projections (Corti et al. 2012; Goddard et al. 2013; Narapusey et al. 2014). The posterior bias correction is useful in the long-term predictions since the

SST biases dominate, which contribute significantly to the model drift. However, the seasonal forecast systems' drift in producing a skillful ISMR depends not only on the ocean component but also on the atmosphere and land components. The process-based understanding of the sources of a CGCM's systematic biases is also highlighted by the necessity of targeting specific improvements in the forecast system for continued improvements in skillful forecasts.

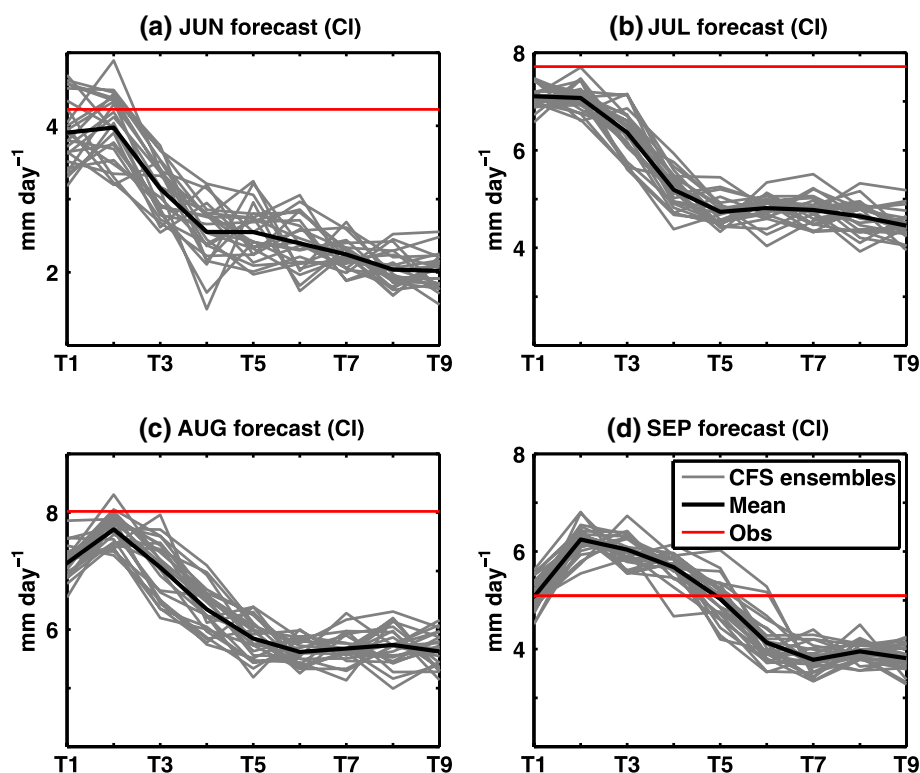
In this study, we explore the role of ocean and atmosphere biases on precipitation biases over Central India (CI) during the boreal summer as forecasted by climate forecast system version 2 (CFSv2) at different lead months. Despite the systematic biases, the long-term simulations of CFS version 1 and the forecast system were shown to have a demonstrable prediction skill for ISMR (Achuthavarier and Krishnamurthy 2010; Chaudhari et al. 2012; Lee Drbohlav and Krishnamurthy 2010). The newer version of the forecast system CFSv2 shows promising skill in reproducing SSTs in IO among other key variables (Saha et al. 2014), although CFSv2 forecasts are still shown to produce systematic dry biases over CI (Goswami et al. 2014).

The goal of this study is to examine the biases in CFSv2 hindcasts and develop a process-level understanding of the interplay between ocean–atmosphere coupled biases and the dry-land bias over CI during the ISM. Throughout this paper, bias refers to the difference of CFSv2 hindcasts produced at different lead times with corresponding observations. The manuscript is organized as follows. The description of the CFSv2 hindcast system used in this study is described in Sect. 2, results are presented and discussed in Sect. 3 and the conclusions are summarized in Sect. 4.

## 2 Description of the forecast system and observational datasets

The monthly mean seasonal forecasts used in this study are from CFSv2 (Saha et al. 2014). The system is initialized each month from January 1982 to March 2011 to produce 9 month-lead forecasts. This system produces 24 ensemble member forecasts in each initialized forecast month, except when initialized in the month of November, which generates 28 members. CFSv2 uses the atmospheric component as NCEP Global Forecast System (GFS) at 0.938° spatial resolution and the ocean component used is Geophysical Fluid Dynamics Laboratory (GFDL) Modular Ocean Model version 4 (MOM4) that has a spatial resolution in the zonal direction of 0.5° and in the meridional direction, 0.25° from 10°S to 10°N, progressively decreasing to 0.5° from 10° to 30°, and is fixed at 0.5° beyond 30° in both hemispheres. In the coupled framework of CFS, the atmosphere and the ocean components exchange freshwater,

**Fig. 1** CFSv2 forecasted precipitation averaged over Central India (16.5°–26.5°N; 74.5°–86.5°E) for **a** June, **b** July, **c** August and **d** September. In all the panels, the red line denotes the observed precipitation. The X-axis shows the month before which the forecast was initialized. For example, in **a**, T5 on X-axis refers to June forecast when the model was initialized 5 months prior (counting includes the forecasted month, i.e., June), which is in February



heat, and momentum fluxes every 30 min during the forecast cycles.

This study uses various sources of observed<sup>1</sup> and reanalysis<sup>2</sup> products in analyzing the biases in CFSv2 hindcasts. Sea-surface temperatures from NOAA-OI-v2 (1982–2011; Reynolds et al. 2002), sub-surface temperatures from ECMWF reanalysis (1982–2011; Balmaseda et al. 2012), 10-m surface winds from CCMP-v3.5 (July 1987–December 2007; Atlas et al. 2011), additional set of 10-m surface winds along with surface latent heat fluxes and surface to the top of the atmosphere winds and specific humidity from CFSR (1979–2009; Saha et al. 2010), precipitations over the ocean (1982–2011) from CMAP (Xie and Arkin 1997) and GPCP (Huffman et al. 2001), and precipitation (1982–2007) over land from APHRODITE (1982–2007; Yatagai et al. 2012) serve as observations. Sub-surface temperatures from CFSR are also tested in addition to the ECMWF product and the conclusions derived in this study are not affected by the choice of the product.

<sup>1</sup> NOAA-OI-v2: National Oceanic and Atmospheric Administration-Optimally Interpolated-version 2

CCMP-v3.5: Cross-Calibrated Multi-Platform—version 3.5

CMAP: Climate Prediction Center Merged Analysis of Precipitation

GPCP: Global Precipitation Climatology Project

APHRODITE: Asian Precipitation—Highly Resolved Observational Data Integration Towards Evaluation.

<sup>2</sup> ECMWF: European Center for Medium-Range Weather Forecasts. CFSR: Climate Forecast System Reanalysis.

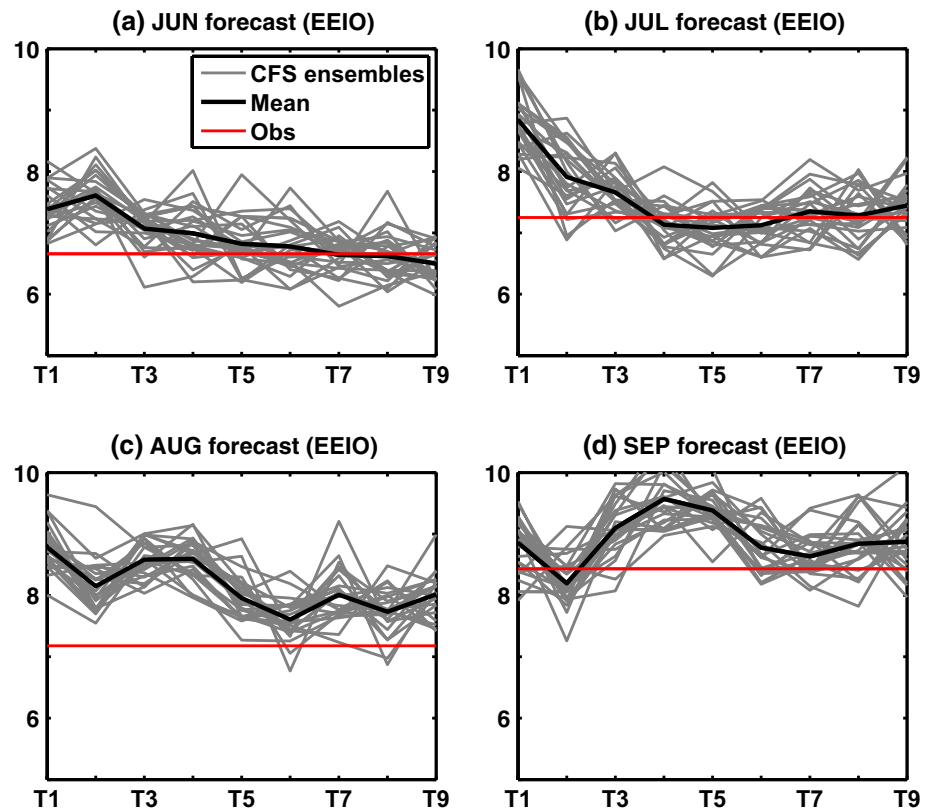
### 3 Results and discussion

#### 3.1 Systematic dry-land biases in CFSv2 JJA forecasts

The CFSv2 forecasts are characterized by a systematic dry precipitation bias over the CI (referred to as dry-land biases hereafter) for June, July and August target months for forecasts initialized individually from various previous months (Fig. 1). The dry-land bias grows systematically in June, July and August forecasts when the system is initialized in earlier months and the bias saturates by the beginning of the spring season. For instance, the bias in the June-forecasted precipitation rapidly grows when the system is progressively initialized in earlier months back to March. Concurrently, the precipitation bias in the eastern equatorial IO is systematically wetter in June to August forecasts as produced by initializing the system at earlier months (Fig. 2). The co-occurrence of a systematic dry bias in the CI and a wet bias in the ocean suggests a large-scale interplay between coupled ocean–atmosphere and land biases.

The mass-flux stream function that accounts for the atmospheric circulation from the surface to top of the atmosphere shows a systematically weaker and diffuse ascending branch of Hadley cell with longer lead-time JJA forecasts (not shown). The progressive weakening of the ascending branch of Hadley circulation in the forecasts corroborates a systematic relationship between the dry-land bias and the concurrent ocean–atmosphere coupled biases.

**Fig. 2** Same as Fig. 1 except that the CFSv2 forecasted precipitation is averaged over the eastern equatorial Indian Ocean ( $5^{\circ}\text{S}$ – $5^{\circ}\text{N}$ ;  $90^{\circ}$ – $110^{\circ}\text{E}$ )



The northward migration of ITCZ during the summer monsoon season that typically starts with an equatorial crossing in April is a key feature in nature and is crucial for the ISMR (Sikka and Gadgil 1980). The precipitation averaged over  $50^{\circ}$ – $70^{\circ}\text{E}$  in the March-initialized CFS forecasts shows excessive precipitation south of  $5^{\circ}\text{S}$  during April and an excess of precipitation north of the equator in May (Fig. 3a). CFSv2 initialized during the rest of spring and early summer months also forecast excess precipitation in the early lead forecasts within  $\sim 10^{\circ}$  latitude around the equator (Fig. 3; panels b–d). The same is also true if the averaging is performed over  $70^{\circ}$ – $90^{\circ}\text{E}$ . The wet biases in the Southern Hemisphere and to the north of the equator are reduced progressively from March to May initialized forecasts up to early summer, while the dry biases progressively increase (decrease) from July to September in the Northern (Southern) Hemisphere.

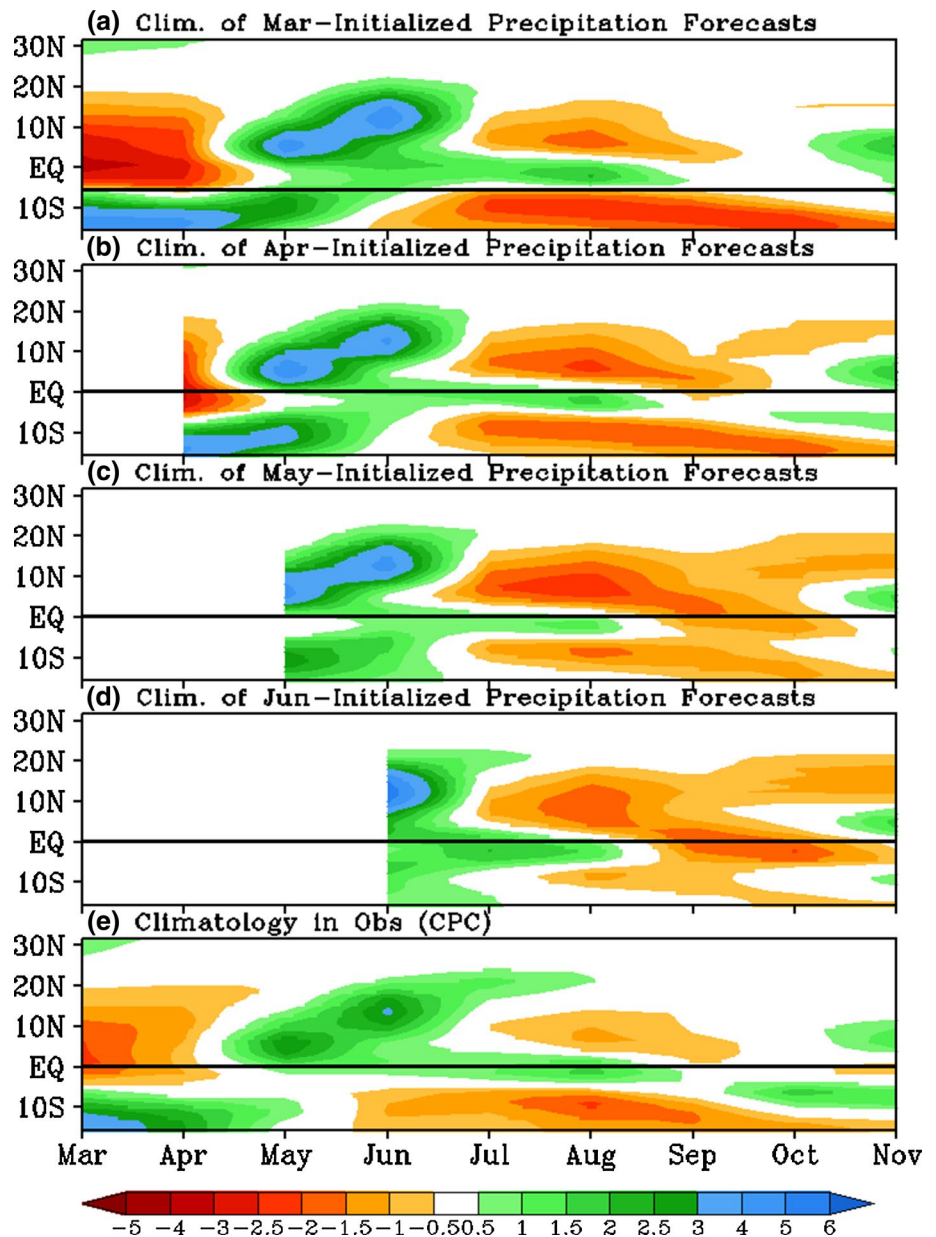
The scatter plot of the biases between the precipitation over CI and the Southern Hemisphere ( $15^{\circ}\text{S}$ – $5^{\circ}\text{S}$ ) suggests the co-occurrence of a majority of the CFSv2 ensemble members precipitating excessively in the Southern Hemisphere in April with a dry-land bias in JJA over CI (Fig. 4a). Generally, a majority of the ensemble members that show excess precipitation in the Southern Hemisphere during the month of April tend to produce a wet bias over

the tropical Indian Ocean ( $5^{\circ}\text{S}$ – $10^{\circ}\text{N}$ ) in the month of May and eventually produce a dry-land bias during summer over CI (Fig. 4b). The chronology of April to May precipitation in the forecasts suggests that the northward migration of the ITCZ is not accurately reproduced by the CFSv2 system and is positively correlated with the dry-land bias in the summer.

### 3.2 Ocean and atmosphere coupled biases

(a) *Spring season* Spring-initialized forecasts develop a systematic pattern of biases throughout the spring season in the IO and the lower atmosphere (Fig. 5). The precipitation biases are mainly confined to the south/southwest IO during early to mid-spring (Fig. 5a, b) and spread to the North IO and the Bay of Bengal (BoB) in late spring (Fig. 5c). During spring, the surface zonal winds (U10 m) exhibit a strong easterly bias over  $5^{\circ}\text{S}$ – $10^{\circ}\text{N}$  and progressively transition to a westerly bias to the south of  $\sim 5^{\circ}\text{S}$ . The strength of the easterly bias grows from March to May to the north of equator in the IO and extends northward of  $10^{\circ}\text{N}$  resulting in a weaker Findlater jet, while the westerly bias diminishes progressively in the southern IO by the end of the spring season (Fig. 5; panels a–c). The biases in

**Fig. 3** Precipitation climatology averaged over 50°–70°E as estimated from March to November forecasts obtained by initializing the model in **a** March, **b** April, **c** May and **d** June. **Panel e** shows the observed climatology (CPC). Note that the long-term annual mean (March–November) is removed from each month



March initialized MAM-averaged forecast show a growth in the systematic pattern wherein the easterly bias strengthens north of equator in the AS and BoB, and an opposite directional bias strengthens around the equator and the Southern Hemisphere (highlighted by solid arrows in Fig. 5d).

The March-initialized forecasts show the growth of warmer SSTs progressively from March to May (Fig. 5, panels e–g). The March forecasts show a warm bias in SSTs (Fig. 5e) primarily originating in three locations: (a) off the coast of Tanzania in the southwest IO (15°–8°S; 40°–50°E), (b) south of the Indian Peninsula and (c) East IO (10°S–Eq. 80°–100°E).

These warm SST biases spread through most part of the IO over 10°S–10°N, AS and BoB by May (Fig. 5; panels f, g).

The reversal of model forecasted winds in the Southern Hemisphere results in warmer SSTs through Ekman pumping acting on the thermocline ridge in this region (Murtugudde et al. 1998; Murtugudde and Busalacchi 1999; Izumo et al. 2008). The Ekman pumping driven by the windstress curl arising from the wind bias in the SWIO induces warmer SSTs in the SWIO in early spring (Figs. 5 and 6). The interannual MAM seasonal-mean correlations between the U10 m averaged in the southwest equatorial IO (SWEIO: 3°S–Eq. 50°–70°E) with the gridded U10 m in the whole region show that the CFS forecasts reproduce

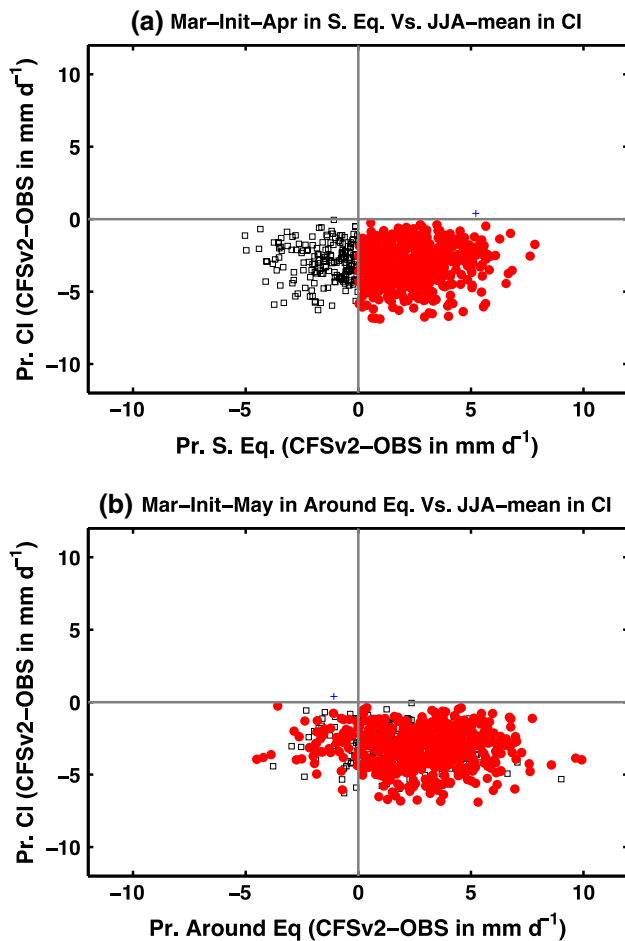


**Fig. 4** Scatter plot between biases in mean summer (JJA) precipitation over Central India (Y-axis) and biases in precipitation (X-axis) during **a** April in the Southern Hemisphere ( $15^{\circ}\text{S}$ – $5^{\circ}\text{S}$ ;  $50^{\circ}$ – $70^{\circ}\text{E}$ ) and **b** May around and to north of the Equator ( $5^{\circ}\text{S}$ – $10^{\circ}\text{N}$ ;  $50^{\circ}$ – $70^{\circ}\text{E}$ ) in March-initialized CFSv2 ensemble forecasts. The scatter points are color coded into three grouped patterns in such a way that in panel **a**, the ensemble members that fall in the first quadrant are colored *blue*, the third quadrant *black* and the fourth quadrant *red*. This color-coding enables us to trace the changes of bias pattern in any particular group of the ensemble members from April (panel **a**) to May (panel **b**)

the spring seasonal wind with a bias over several regions. In the observations, the seasonal mean U10 m in SWEIO is positively correlated in the IO, AS and BoB (Fig. 6a), whereas the March-initialized spring forecasts show that the seasonal mean U10 m in SWEIO is anti-correlated with U10 m to the south of the equator, and in northern AS and BoB (Fig. 6b), which explains the preferential drift of winds in spring.

The wind speed ( $\sqrt{u^2 + v^2}$ ) biases at 10 m above the surface show that the wind speed is weaker for the March to April forecasts and stronger in May forecasts in the SWIO, AS and BoB (Fig. 7; panels a, b). The reduced (increased) latent heat fluxes in the spring season are coherent with the

reduced (increased) wind speed biases (Fig. 7) and warmer (colder) SST biases (Fig. 5). The weaker wind speed and reduced net latent heat flux during the early to mid-spring accelerates the SST warming in spring (Fig. 5; panels e–h). The warm SST bias developed in the WEIO due to the wind biases grow systematically from April to May (Fig. 5; panels f, g) leading to an excessive precipitation to the north of WEIO, which in turn has a positive feedback to the winds and thus exacerbates the easterly wind bias in that region.

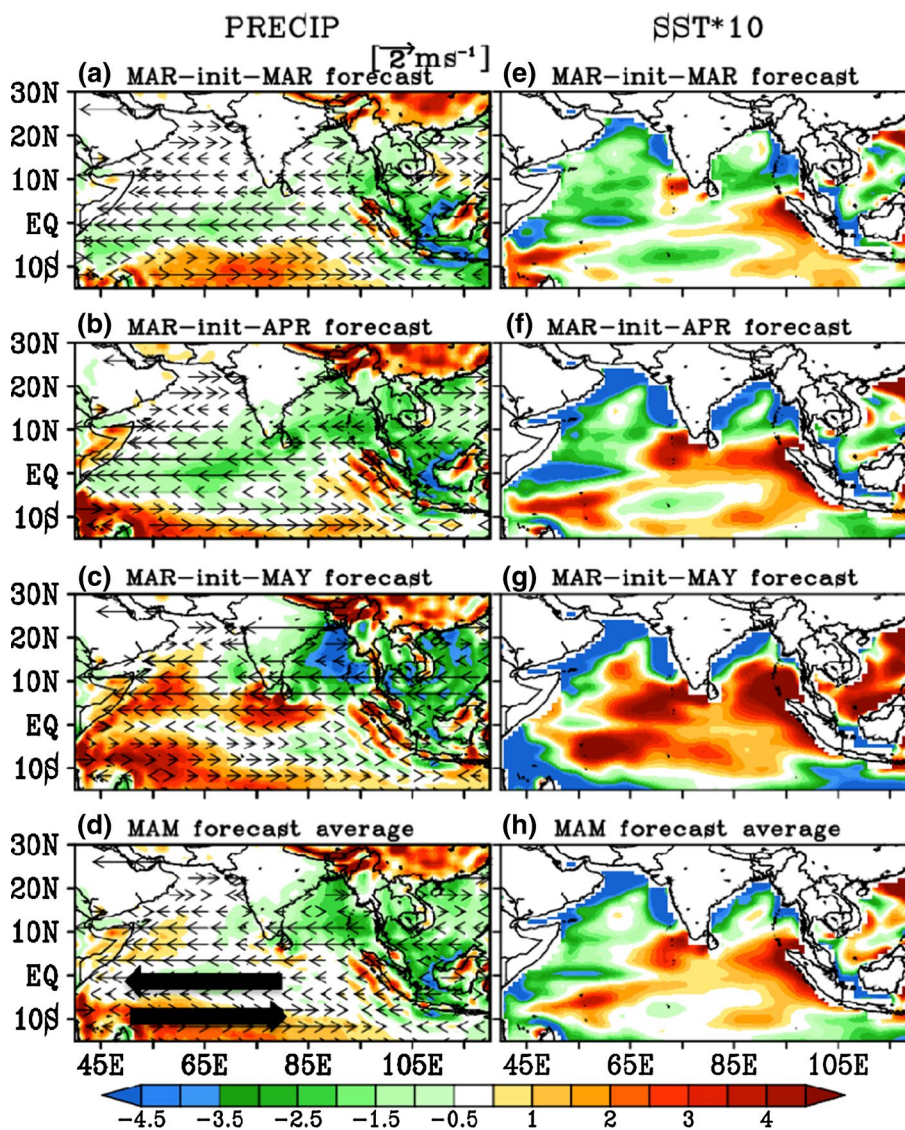
The spring forecasted  $20^{\circ}\text{C}$  isotherm (D20 hereafter) differs systematically from observations. The March-initialized March to November forecasts show that during the spring season, D20 deepens in the SWEIO compared to observations (Fig. 8). The same is also true for April initialized forecasts. The systematic build-up of a mean thermocline bias, examined with the depth of the D20 in the SWIO, is a result of enhanced Ekman pumping and acts to sustain the warm SST bias.

(b) *Summer season* The U10 m bias in the summer months is exactly opposite to the bias in spring. In summer, the CFSv2 wind biases over the ocean are predominantly westerly with a weak but a systematic easterly bias pattern northward of  $\sim 10^{\circ}\text{N}$  in the AS and off the west coast of India. The complete reversal of wind biases in summer redistributes the precipitation biases over the entire basin and has been affected by their mutual feedbacks.

The June forecasts initialized in the months from March to June show higher than observed precipitation in the AS and off the west coast of India (Fig. 9; panels a–d). In general, the March-to-June-initialized model forecasts show that the CFSv2 produces excess precipitation in the SWEIO and the AS compared to observations. The strong westerly wind bias off the Somali coast in conjunction with the easterly bias in northern AS produces a large-scale cyclonic circulation that results in the high precipitation off the west coast of India in the June forecasts (Fig. 9; panels a–d). Higher than observed precipitation during the early summer in the AS and off the coast of western India feeds back to the winds in the region during mid-to-late summer by producing anomalous winds that weaken the Findlater jet leading to an easterly bias over northern AS (Fig. 9; panels e–h). The anomalous strengthening of easterly bias from mid to late summer in the northern AS dissipates the large-scale cyclonic system set-up during the early summer and terminates the wet bias over the AS (Fig. 9; panels e–l).

Coherent with the westerly wind bias, the positive wind speed bias off the Somali coast induces enhanced latent heat losses from the ocean that increase the moisture availability to the large-scale cyclonic system in the AS and off the west coast of India in the early summer

**Fig. 5** Biases in precipitation (color shades in  $\text{mm day}^{-1}$ ) and 10-m zonal wind (arrows in  $\text{m s}^{-1}$ ) in March initialized **a** March, **b** April, **c** May and **d** Mar–Apr–May averaged forecasts. The solid black arrows in panel **d** indicate the strengthening biases in opposing directions in the southern Indian Ocean. SST biases ( $\times 10^\circ\text{C}$ ) in March initialized March, April, May and Mar–Apr–May forecasts are shown in panels **e**, **f**, **g** and **h**, respectively



forecasts (Fig. 10; panels a–d). In the mid-to-late summer, the positive wind speed and the latent heat flux biases systematically get stronger in the EEIO and BoB and contribute to the wet bias in those regions (Fig. 10; panels e–l).

The delay in the equatorial crossing of the ITCZ in April and May forecasts (Figs. 3 and 4), significantly impacts the ISMR. In the mid-to-late spring forecasts the wind bias in the Southern Hemisphere generates a stronger windstress curl, which in turn produces warmer SSTs in the SWIO through Ekman pumping (Fig. 5). The warmer SSTs lead to anomalous precipitation and the position of the ITCZ is pushed southward compared to the observations in late spring. This particular feature of the delay in the equatorial crossing of the ITCZ is similar to the processes explained by Murtugudde et al. (1998) and Izumo et al. (2008), except that the time required for the build-up of warmer

SSTs in the SWIO and the AS is much shorter because, (1) the positive bias in the Ekman pumping is rapidly set-up by the surface wind bias during spring and (2) weaker surface wind-speed and latent heat flux biases exacerbate the warm SST bias. Briefly, the wind bias in the southwestern IO enhances the annual Rossby wave and surface warming which is associated with a weaker Findlater jet and a weaker Indian monsoon. But Murtugudde et al. (1998) and Izumo et al. (2008) did not focus on the consequences of the IO warming on local precipitation and the impacts on the cross-equatorial vertically integrated moisture transport (VIMT) and the potential land–ocean competition for rainfall.

The other common feature of the summer precipitation bias over the ocean is found in the central to eastern equatorial IO. This wet-bias is stronger in the central equatorial IO in the early summer and propagates to the east

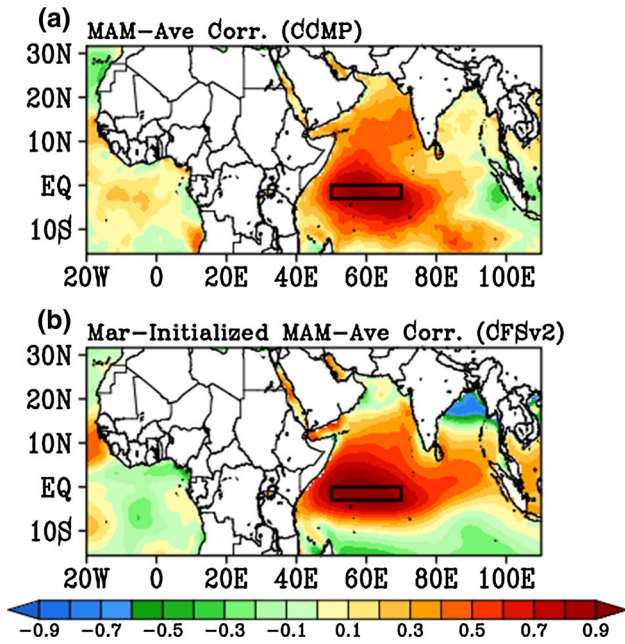
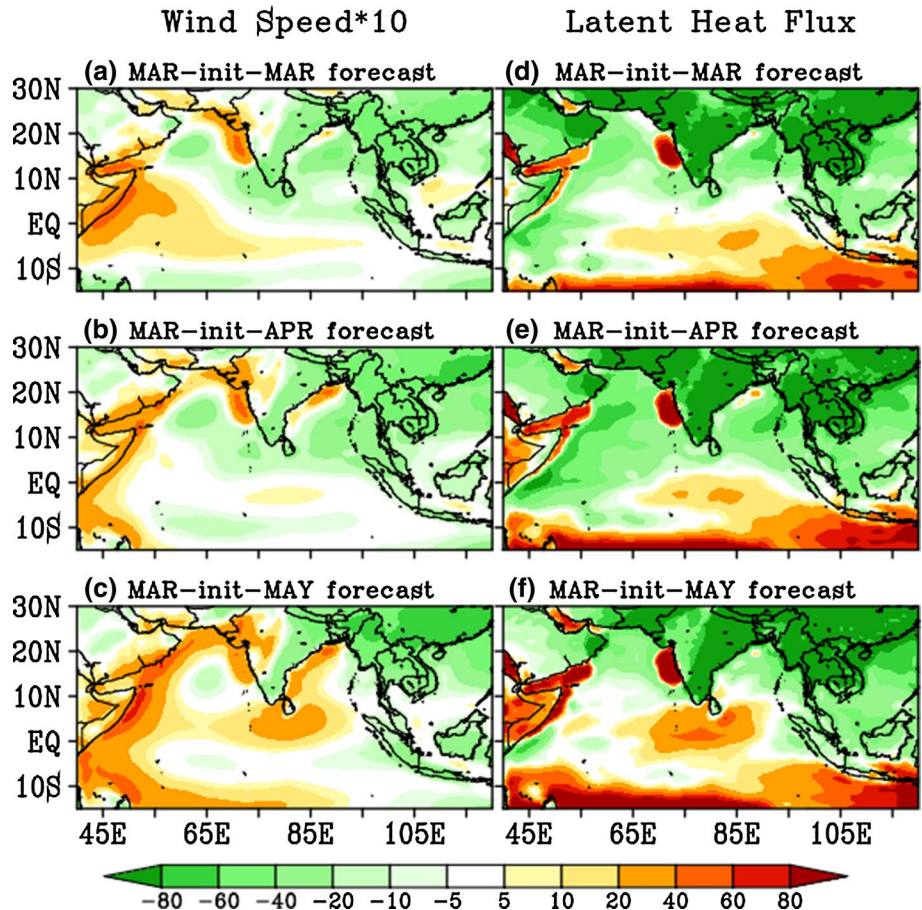


**Fig. 6** Interannual correlation between 10-m zonal wind component in the *rectangular box* comprised of the area 3°S-Eq, 50°–70°E with the rest of the region in the spring season shown for **a** CCMP winds and **b** March initialized model forecasts

**Fig. 7** Biases in March initialized March, April, and May forecasts for 10-m wind speed ( $\sqrt{u^2 + v^2}$ ; in  $\text{ms}^{-1}$ ) shown in *panels a, b and c*, respectively, and for surface latent heat flux (in  $\text{W m}^{-2}$ ) in *panels d, e, and f*, respectively



from June to August. In summer, the westerly wind bias strengthens the downwelling Kelvin wave and thereby the movement of precipitation bias from central to eastern equatorial IO (Figs. 9 and 11a).

The amplitude of D20’s quasi-annual harmonic averaged over 3°S-Eq in the March initialized March to November forecasts highlights the Kelvin wave propagation from SWEIO in late spring to EEIO in summer (Fig. 11a). The quasi-annual harmonic is computed by continuously arranging each of the 1982–2011 March-initialized March to November forecasts ( $30 \times 9$  months) and regress the data onto a harmonic fixed at a period of 9 months ( $P = 1$  in the Eq. (3) of Narapusetty et al. 2009). The sum of first four harmonics is exactly equivalent to the climatological average of forecasts separated by a fixed phase of 9 months (March–November forecasts) and the data associated with the first harmonic captures the March-to-November variability. A similar equatorial Kelvin wave propagation during spring-summer is missing in the observations; the quasi-annual harmonic from the March to November pooled data from CFSR shows a much shallower thermocline (weaker D20) in SWEIO compared to CFSv2 forecasts and the communication is missing between SWEIO and EEIO due to the absence of the Kelvin wave propagation as seen in



**Fig. 8** Thermocline climatology depicted from March to November in **a** observations (ECMWF) and **b** March-initialized CFSv2 forecasts. *Red oval in panel b highlights the deeper thermocline in SWEIO during spring in the CFSv2 forecasts*

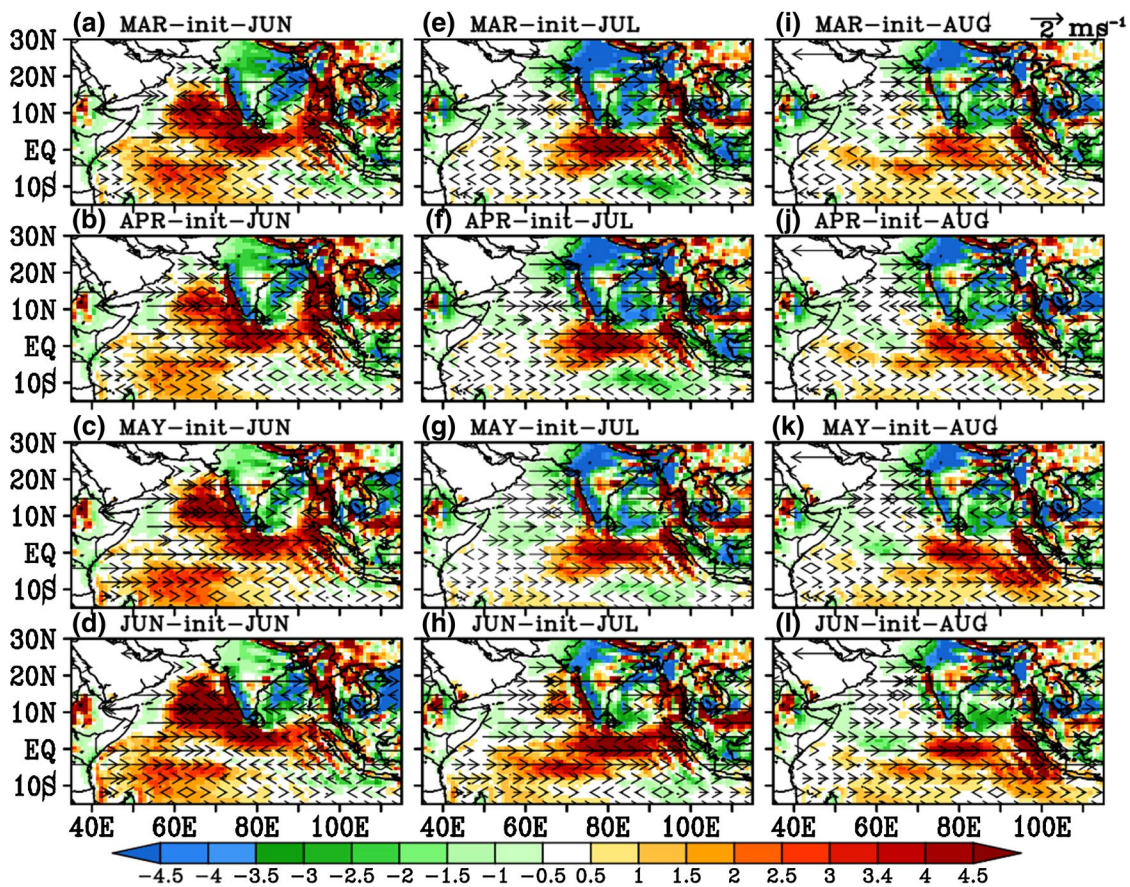
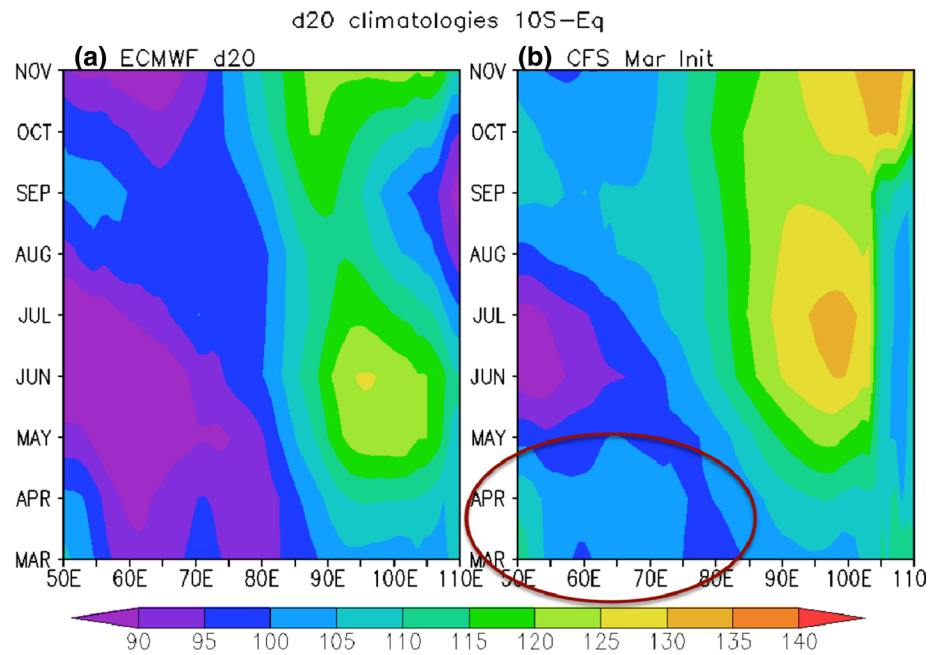


**Fig. 9** Biases in precipitation (*color shades* in  $\text{mm day}^{-1}$ ) and 10-m zonal-wind ( $\text{m s}^{-1}$ ) as obtained by initializing CFSv2 in March, April, May and June months to forecast June as depicted in the *panels a–d*, July in *e–h*, and August in *i–l*

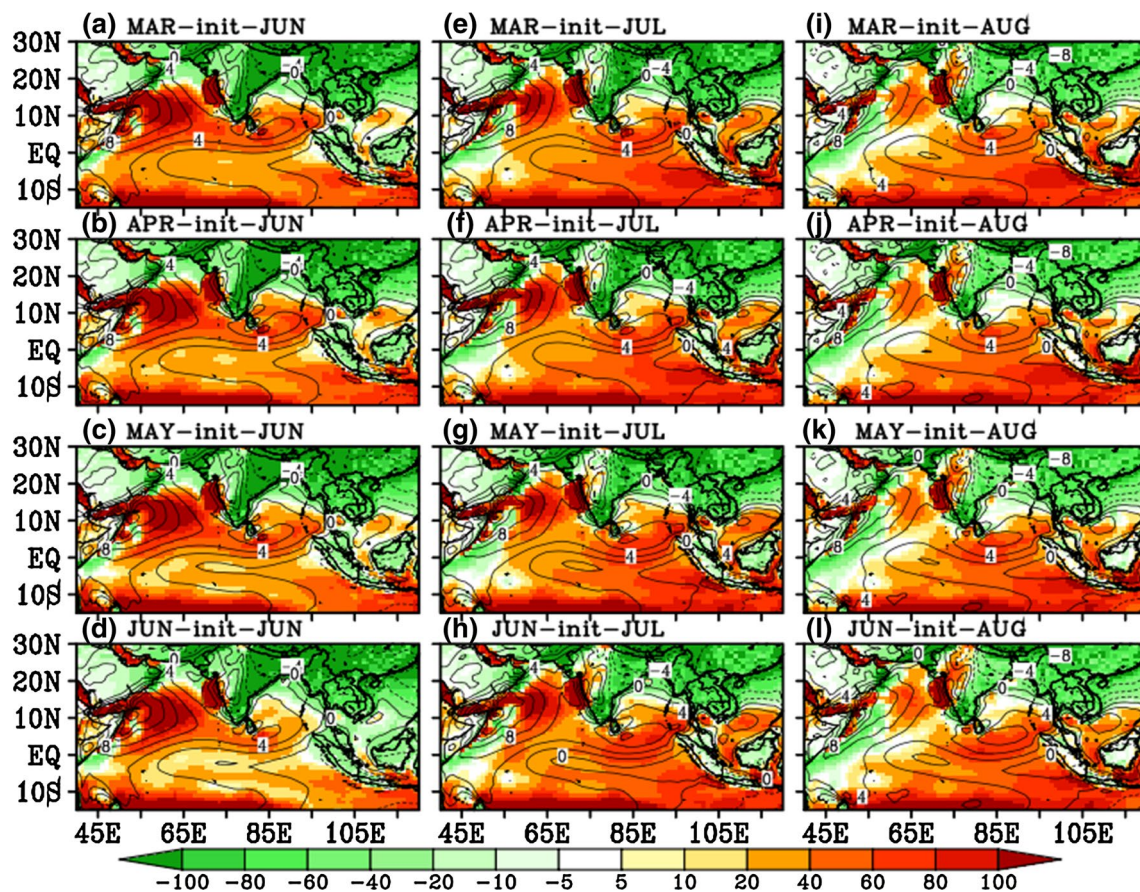


**Fig. 10** Biases in surface latent heat flux (color shades in  $\text{W m}^{-2}$ ) and wind speed ( $\sqrt{u^2 + v^2}$ ; contours in  $\text{ms}^{-1}$ ) as obtained by initializing CFSv2 in March, April, May and June months to forecast June as depicted in the panels a–d, July in e–h, and August in i–l

CFSv2 (Fig. 11b). The quasi-annual propagation in CFSR is produced mainly through a westward moving Rossby wave in the south equatorial IO.

The westerly wind bias over the equatorial IO strengthens the downwelling Kelvin wave which continues as coastal Kelvin waves at the eastern boundary (Sumatra) and eventually the Kelvin wave energy is dispersed into Rossby waves and propagate westward on either side of the equator (Fig. 12). The  $3^\circ\text{--}6^\circ\text{N}$  averaged quasi-annual D20 harmonic reveals that in the CFSv2 forecasts, the dispersed Rossby wave propagation off the Sumatran coast is much stronger in summer compared to CFSR (compare Fig. 12 panels a, b). In CFSR, the Rossby wave activity starts in the beginning of spring and peaks in mid-summer, whereas in the CFSv2 forecasts, much stronger Rossby wave activity is produced from the beginning of summer and extends beyond August due to the available energy from a stronger downwelling Kelvin wave.

Similar to the Northern Hemisphere, the presence of a stronger Rossby wave in CFSv2 starting from summer is attributed to the existence of Kelvin wave activity and the associated dispersed Rossby wave in the southern

equatorial IO. On the other hand, the CFSR data is marked with Rossby wave propagation from mid-spring (Fig. 12). In the Southern Hemisphere, Rossby wave activity is stronger in CFSR (Fig. 12d) due to the non-dispersive quasi-annual Rossby wave propagation as observed in nature from the southeastern corner of the southern tropical IO (Masumoto and Meyers 1998); on the other hand, this non-dispersive Rossby wave pattern is obstructed by the downwelling Kelvin wave in the CFSv2 forecasts due to the westerly wind bias in summer resulting in a weaker Rossby wave activity (Fig. 12c).

The VIMT as estimated by  $\int_{1000\text{hpa}}^{300\text{hpa}} q|\vec{v}| dp$ , where  $q$  is the specific humidity and  $|\vec{v}|$  is magnitude of the wind vector calculated as  $\sqrt{u^2 + v^2}$ , shows that the bias in moisture transport systematically increases from June to August in the equatorial IO along the track of the downwelling Kelvin wave (Fig. 13). The positive VIMT bias in the IO is coherent with the positive precipitation biases in the tropical IO and BoB (compare Figs. 9 and 13). The colder SSTs due to the enhanced latent heat loss from late spring to summer over the AS lowers the moisture availability (Levine and Turner 2012; Levine et al. 2013; Sahana et al. 2015).

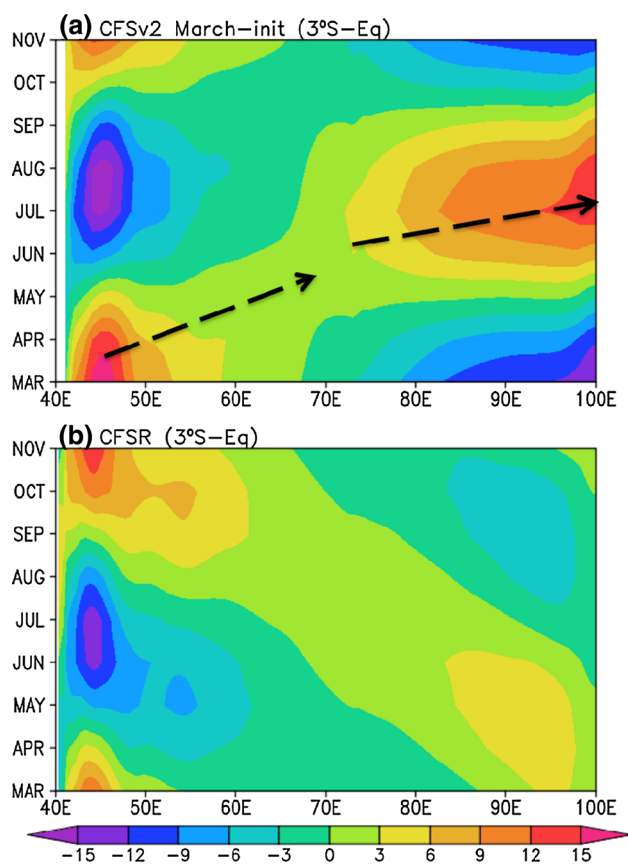


**Fig. 11** Hovemuller diagram depicting the amplitude of D20's quasi-annual harmonic averaged over Eq–3°S from March to November in **a** the March-initialized CFSv2 forecasts and **b** CFSR

The resulting reduced VIMT in conjunction with weakened Findlater jet reduces the moisture supply in the monsoonal flow over CI. The analysis presented in this study indicates that the positive (negative) VIMT bias over EEIO (CI and AS) is mainly due to the local warmer (colder) SSTs, which are themselves a result of the large-scale SST bias coupled with the wind and precipitation biases and the associated feedbacks. However, the strength of the VIMT bias could partly be sensitive to the entrainment and detrainment rates of the convective parameterization (Bush et al. 2015) employed in the CFSv2. The sensitivity to convective parameterization, especially in terms of terrestrial and marine convection, is a natural extension of the present study but is beyond the scope of numerical experiments analyzed in this study.

To understand how the biases in the BoB are correlated with precipitation over India over the extended summer monsoon season (JJAS), four sub-domains (east, west, north and south) are chosen in the BoB and the mean JJAS precipitation in those sub-domains is correlated with the gridded precipitation over a larger region comprising of land (much of the sub-continent) and ocean (IO and BoB;

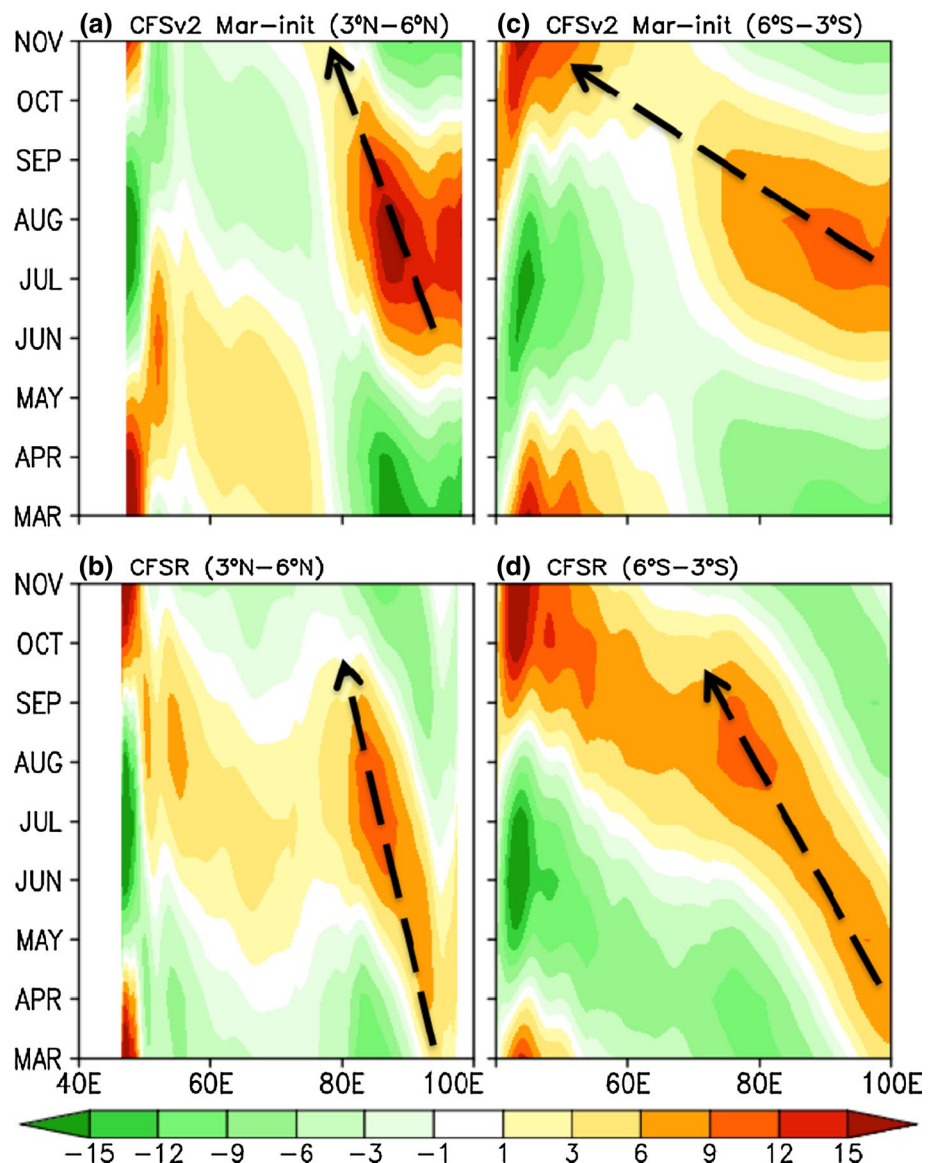
Meehl et al. 2012). The key goal of this correlation analysis is to provide insights into the extent to which the downwelling Kelvin wave bias originating in the equatorial IO can influence the SST in the BoB and thereby alter the precipitation over the entire region. This analysis also helps in understanding the preferred paths of monsoon propagation in CFSv2 forecasts from equatorial Indian Ocean/mouth of BoB to the Himalayan foothills.

In the observations, precipitation averaged over the eastern BoB is positively correlated over CI (Fig. 14; panel c). Precipitation over the northern box (panel a) is negatively correlated over most of India except for a weak positive correlation over the central part. The precipitation over the western (eastern BoB to the south India) and southern (near EEIO) BoB are negatively correlated with the precipitation over CI (panels b, d, respectively). The preferred northwestern propagation of correlations highlights the intra-seasonal component of the monsoonal flow, indicating that the cyclonic storms and depressions that form in the central east and west BoB are most likely to contribute to the active precipitation events over CI through northwestward propagation. The stronger seesaw structure of the correlations between the northern BoB extending to the northern India and southern BoB extending to the EEIO suggests an intensification of the local Hadley cell plays an important role (Slingo and Annamalai 2000).

In contrast to the observations, the long-lead forecasts (for ex., the April-initialized JJAS forecasts), exhibit two distinctive correlation patterns: (1) precipitation in each of the north (Fig. 15a), west (Fig. 15b) and east BoB (Fig. 15c) regions is predominantly anti-correlated with precipitation over the equatorial IO, consistent with the local Hadley circulation bias, and (2) precipitation over CI is strongly anti-correlated with precipitation over southern BoB (Fig. 15d), highlighting the impact of the systematic thermocline bias induced by the Rossby wave mentioned above (Fig. 12a). The stronger Rossby wave activity to the north of the equator in the CFSv2 forecasts increases heat content in the BoB during summer as discussed in Krishnan et al. (2006). Also, the long-lead JJAS forecasts lack the northwestward tilt in the correlations that is commonly found in observations (compare panels a, b, d of Fig. 15 with respective panels in Fig. 14).

These differences in the correlation patterns diminish with shorter lead-time JJAS forecasts; for instance, the correlation patterns in the June initialized JJAS forecasts are closer to observations (Fig. 16) albeit with the exception of northwestward tilt. The systematic westerly wind bias in the north equatorial IO/BoB during summer is the source of the Rossby wave strength and this strength is fueled by the westerly wind bias that increases with forecast lead-time. The resulting warmer SST bias systematically grows in the long-lead forecasts and exacerbates the dry-land bias by

**Fig. 12** Hovemuller diagrams depicting amplitude of D20's quasi-annual harmonic for March-initialized CFSv2 forecasts in *panels a* and *c*, and CFSR results in *panels b* and *d*. The *arrows* in all the *panels* indicate direction of the wave propagation.



altering the local Hadley circulation. This is evident in the contrast of April-initialized JJAS forecasts with the June-initialized JJAS forecasts, with the latter showing weaker negative correlations between precipitations averaged in the southern sub-domain of the BoB and precipitation over CI (compare Fig. 16d with Fig. 15d).

#### 4 Conclusions

The main goal of this study is to examine the phenology of biases in CFSv2 hindcasts and acquire a process-level understanding of the interplay between coupled ocean–atmosphere processes and the dry-land bias over Central India during the Indian summer monsoon. The spring-initialized CFSv2 forecasts are marked by systematic warm

SST biases in the southwestern IO and the AS due to (1) Ekman pumping induced by wind biases and (2) weaker wind speed and latent heat flux biases at the surface.

The spatial pattern of seasonal-mean zonal wind hindcasts produced in the Southern Hemisphere is particularly interesting since the wind direction changes from predominantly easterly in the equator–5°S band to westerly in the 5°–15°S band on interannual timescales. This opposing wind structure is projected onto the mean wind bias, which in turn leads to enhanced Ekman pumping in the southwestern IO. A comprehensive understanding of the wind bias initiation requires further sensitivity experiments and will be reported elsewhere. But the process understanding of the evolution of wind bias growing into coupled ocean–atmosphere processes that amplify the seasonal features

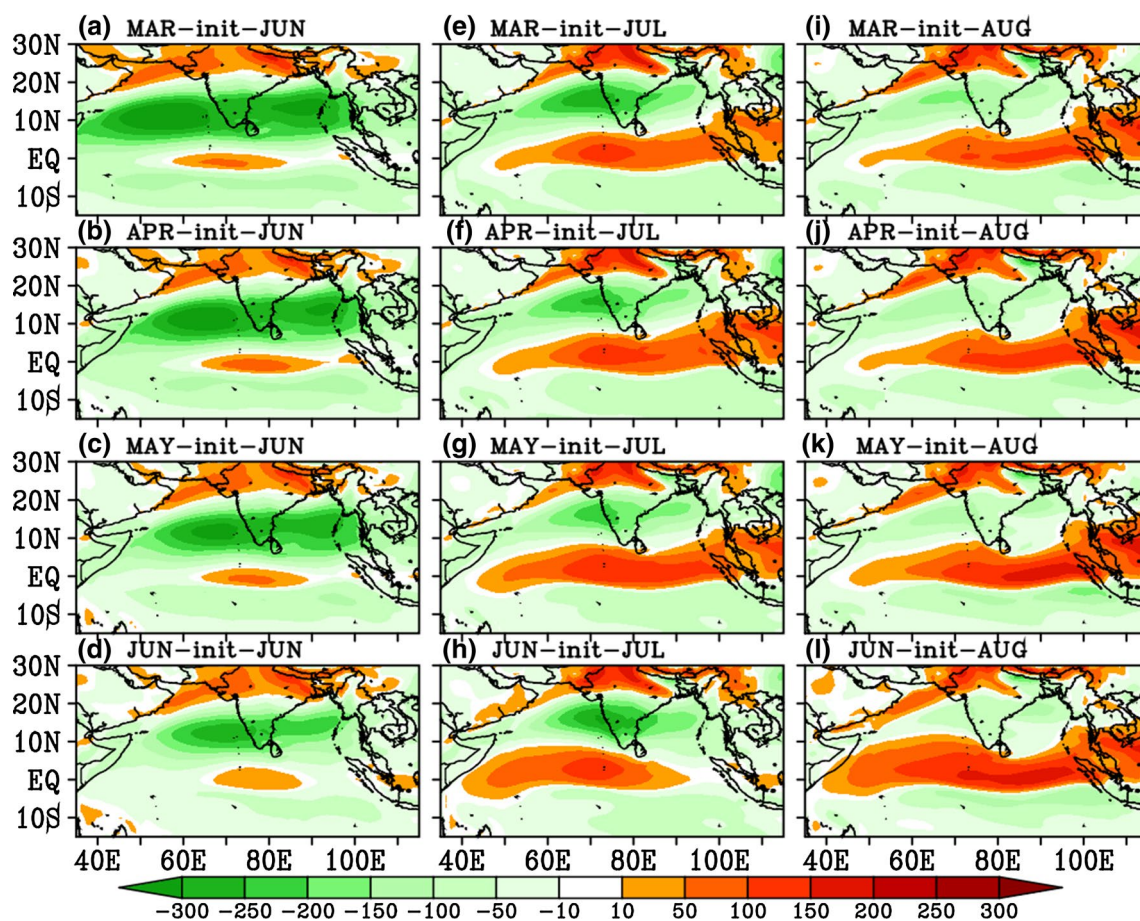


**Fig. 13** Similar to Fig. 10, except that the biases are shown for vertically integrated moisture transport (in  $\text{kg m}^{-1} \text{s}^{-1}$ )

highlighted in this study is important for designing those sensitivity experiments.

The buildup of warmer SSTs in association with a deeper thermocline in the southwest IO inhibits the northward propagation of ITCZ during April. Beyond this deficiency in the forecasts, two key ocean–atmosphere coupled mechanisms are identified; one in the AS and the other in the eastern equatorial IO that explain the systematic dry-land and wet-ocean biases occurring concurrently in the summer. The processes involved are as follows. A systematic positive curl in the low-level winds during the month of June over the AS in conjunction with the anomalous Ekman pumping (to the north of  $5^\circ\text{N}$ ) produces excess precipitation over central AS and eventually leads to a depletion of moisture in the Findlater jet. In the equatorial IO, the shift of wind bias from easterly in spring to westerly in summer leads to a strengthened downwelling Kelvin wave that deepens the thermocline in the eastern IO. The deeper thermocline and warm SST biases induce a wet bias in the equatorial IO and a dry bias over CI and thus alter the local Hadley circulation. The Kelvin wave activity also produces reflected Rossby waves off the coast of Sumatra and induces positive SST

and precipitation biases in the eastern and the southern BoB, which reinforce the changes in the local Hadley circulation.

It should be reemphasized that this is the first step in diagnosing the precipitation biases over the IO sector and should be considered with the caveat that attribution of cause and effect is always subject to the chicken and egg conundrum in a coupled system. The application of flux and SST bias-correction techniques during the forecast system integrations is shown to improve the extended range rain forecasts by Abhilash et al. (2013) and Borah et al. (2015). However, such an analysis is beyond the scope of the current study since the main aim here is to highlight process biases producing a dry land bias at seasonal timescales. The role of external influences from the heat sources in the other tropical oceans and the role of the global processes such as the ITCZ which is a trans-tropical conveyor belt of subseasonal to interannual variability cannot easily be analyzed. Further analysis to explore such external influences is underway; e.g., in the context of studies that report a relation between the Atlantic equatorial warming and the monsoon depressions (Pottapinjara et al. 2014) and the influence of the Indonesian throughflow on the heat

**Fig. 14** Correlations between area-averaged JJAS mean precipitations in various sub-domains as depicted in **a–d** with the gridded precipitation over the entire area in GPCP observations

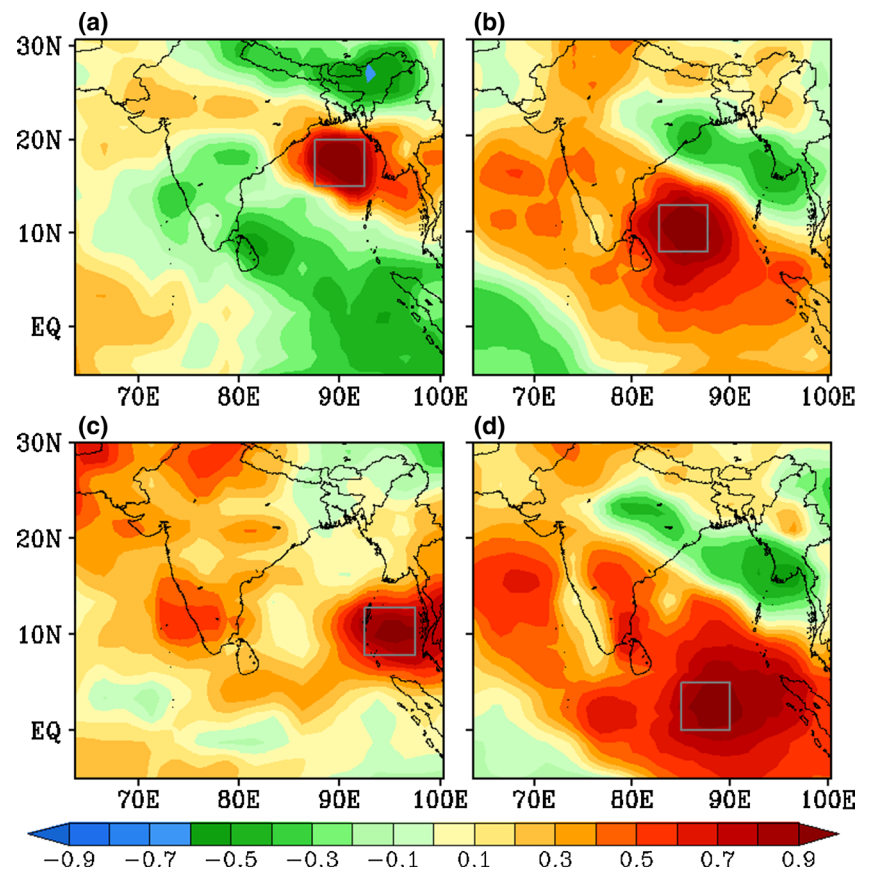


**Fig. 15** Same as in Fig. 14, but for April-initialized JJAS forecasts in CFSv2

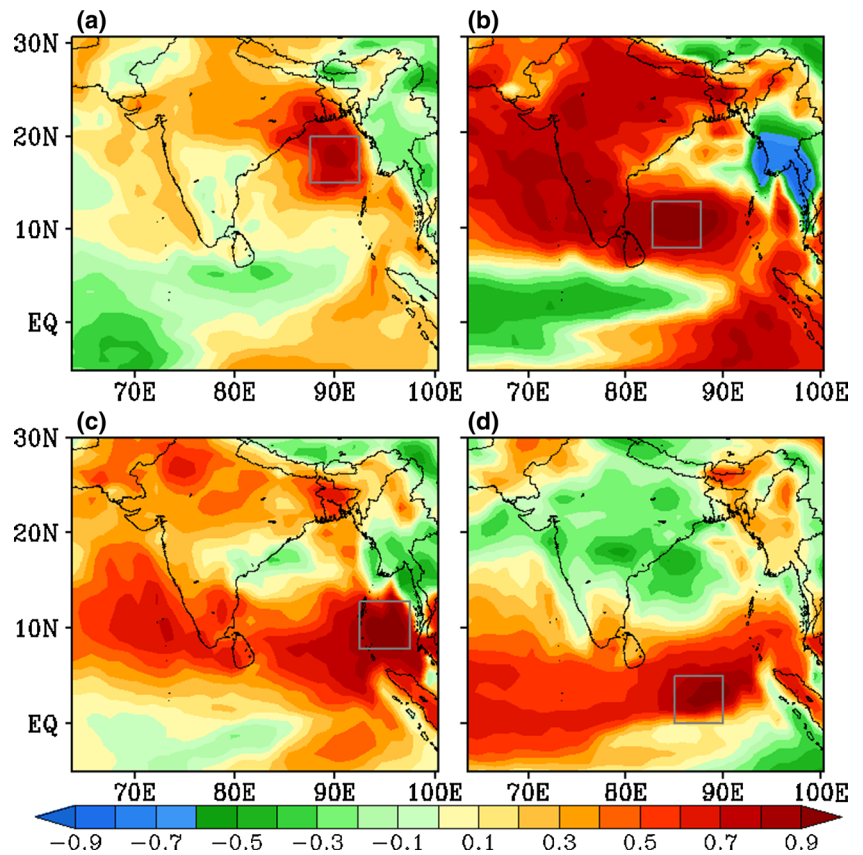
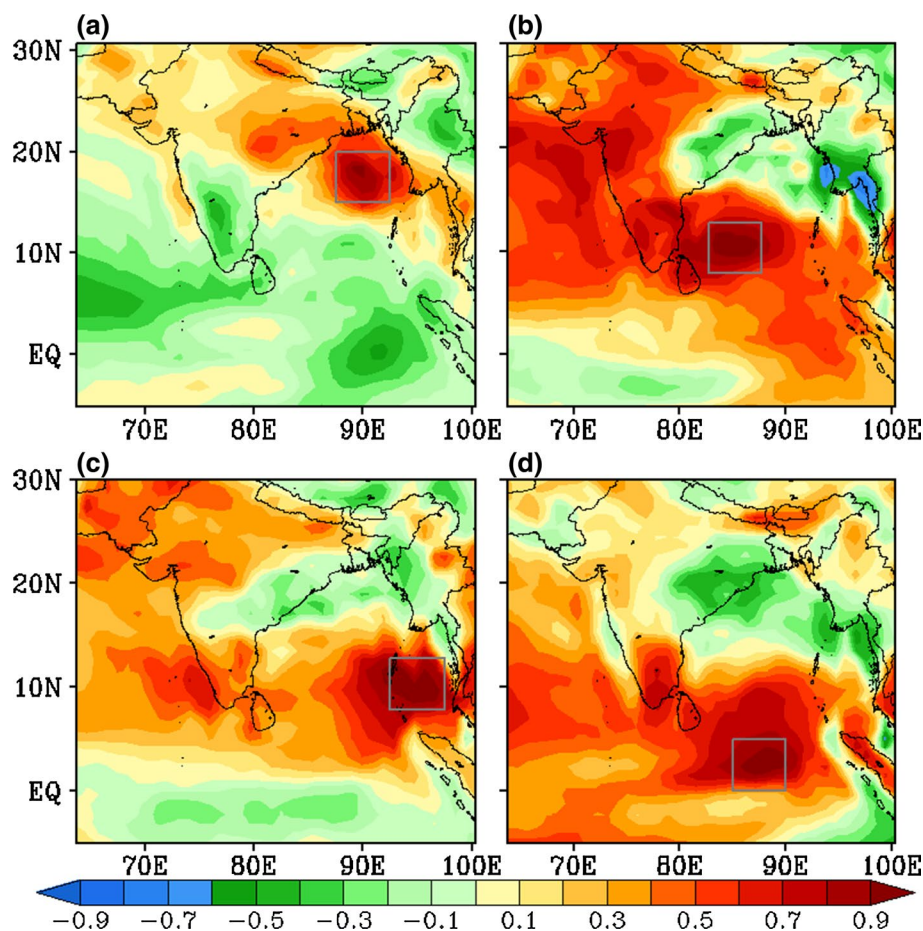


**Fig. 16** Same as in Fig. 15, but for June-initialized JJAS forecasts in CFSv2



budget in the southwestern IO (Zhou et al. 2008a, b, 2010). We should also note that the equatorial-crossing of the rainbands and the ISM are intrinsically intraseasonal processes and the relation between the eastward and northward propagating systems (Zhou and Murtugudde 2014) and their renditions in model forecasts are bound to play a critical role in the dry-land bias (Goswami et al. 2014). The delay in the northward propagation of ITCZ is hypothesized as a competition between equatorial and continental convergence zones during summer monsoon (Gadgil and Sajani 1998). The sensitivity of equatorial crossing to the convective parameterization scheme could also shed light on the strength and the extent of biases in low-level circulation and moisture availability over the equatorial convergence zone, north of WEIO and AS (Bush et al. 2015).

The prediction skill of ISMR, among the other factors, depends on model's ability to capture the contrasts in diurnal cycle of convection over the ocean and land (Yang and Slingo 2001) along with the ability to reproduce the organized convection over the Maritime continent (Neale and Slingo 2003). Therefore examining the CFSv2 forecast system at sub-daily scales should provide further information on the role of physical parameterizations in developing

systematic biases. These will also be explored further and the findings will be reported elsewhere.

**Acknowledgments** The authors gratefully acknowledge the financial support given by the Earth System Science Organization, Ministry of Earth Sciences, Government of India (MM/SERP/Univ\_Maryland\_USA/2013/INT-16/002) to conduct this research under Monsoon Mission. The authors also acknowledge Dr. Krishnan, Dr. Rajeevan, Dr. Shukla, and Dr. Kinter for helpful comments and discussions.

**Open Access** This article is distributed under the terms of the Creative Commons Attribution 4.0 International License (<http://creativecommons.org/licenses/by/4.0/>), which permits unrestricted use, distribution, and reproduction in any medium, provided you give appropriate credit to the original author(s) and the source, provide a link to the Creative Commons license, and indicate if changes were made.

## References

- Abhilash S, Sahai AK, Borah N, Chattopadhyay R, Joseph S, Sharmila S, De S, Goswami BN (2013) Does bias correction in the forecasted SST improve the extended range prediction skill of active-break spells of Indian summer monsoon rainfall? *Atmos Sci Lett* 15:114–119. doi:10.1002/asl2.477

- Abhilash S, Sahai AK, Borah N, Chattopadhyay R, Joseph S, Sharmilla S, De S, Goswami BN, Kumar A (2014) Prediction and monitoring of monsoon intraseasonal oscillations over Indian monsoon region in an ensemble prediction system using CFSv2. *Clim Dyn* 42:2801–2815. doi:[10.1007/s00382-013-2045-9](https://doi.org/10.1007/s00382-013-2045-9)
- Achuthavarier D, Krishnamurthy V (2010) Relation between intraseasonal and interannual variability of the south Asian monsoon in the National Centers for Environmental Predictions forecast systems. *J Geophys Res*. doi:[10.1002/joc.3489](https://doi.org/10.1002/joc.3489)
- Atlas R, Hoffman RN, Ardizzone J, Leidner SM, Jusem JC, Smith DK, Gombos D (2011) A cross-calibrated, multiplatform ocean surface wind velocity product for meteorological and oceanographic applications. *Bull Am Meteorol Soc* 92:157–174. doi:[10.1175/2010BAMS2946.1](https://doi.org/10.1175/2010BAMS2946.1)
- Balmaseda MA, Mogenssen K, Weaver AT (2012) Evaluation of the ECMWF ocean reanalysis system ORAS4. *R Meteorol Soc, Q. J.* doi:[10.1002/qj.2063](https://doi.org/10.1002/qj.2063)
- Borah N, Sahai AK, Chattopadhyay R, Joseph S, Abhilash S, Goswami BN (2013) A self-organizing map based ensemble forecast system for extended range prediction of active/break cycles of Indian summer monsoon. *J Geophys Res Atmos* 118:1–13. doi:[10.1002/jgrd.50688](https://doi.org/10.1002/jgrd.50688)
- Borah N, Sahai AK, Abhilash S, Chattopadhyay R, Joseph S, Sharmila Kumar A (2015) An assessment of real-time extended range forecast of 2013 Indian summer monsoon. *Int J Climatol* 35:2860–2876. doi:[10.1002/joc.4178](https://doi.org/10.1002/joc.4178)
- Bush SJ, Turner AG, Woolnough SJ, Martin GM, Klingaman NP (2015) The effect of increased convective entrainment on Asian monsoon biases in the MetUM general circulation model. *Q J R Meteorol Soc* 141:311–326. doi:[10.1002/qj.2371](https://doi.org/10.1002/qj.2371)
- Chaudhari HS, Pokhrel S, Saha SK, Dhakate A, Yadav RK, Salunke K, Mahapatra S, Sabeerali CT, Rao SA (2012) Model biases in long coupled runs of NCEP CFS in the context of Indian summer monsoon. *Int J Climatol* 33:1059–1063. doi:[10.1002/joc.3489](https://doi.org/10.1002/joc.3489)
- Corti S, Weisheimer A, Palmer T, Doblas-Reyes F, Magnusson L (2012) Reliability of decadal predictions. *Geophys Res Lett* 39:L21712. doi:[10.1029/2012GL053354](https://doi.org/10.1029/2012GL053354)
- DelSole T, Shukla J (2012) Climate models produce skillful predictions of Indian summer monsoon rainfall. *Geophys Res Lett* 39:L09703. doi:[10.1029/2012GL051279](https://doi.org/10.1029/2012GL051279)
- Gadgil S, Sajani S (1998) Monsoon precipitation in the AMIP runs. *Clim Dyn* 14:659–689. doi:[10.1007/s003820050248](https://doi.org/10.1007/s003820050248)
- Gadgil S, Rajeevan M, Nanjundiah R (2005) Monsoon prediction—why yet another failure? *Curr Sci* 88:1389–1400
- Goddard L, Kumar A, Solomon A, Smith D, Boer G et al (2013) A verification framework for interannual-to-decadal predictions experiments. *Clim Dyn* 40:245–272. doi:[10.1007/s00382-012-1481-2](https://doi.org/10.1007/s00382-012-1481-2)
- Goswami BB, Deshpande M, Mukhopadhyay P, Saha SK, Rao SA, Murthugudde R, Goswami BN (2014) Simulation of Indian summer monsoon intraseasonal oscillation variability in NCEP CFSv2 and its role on systematic bias. *Clim Dyn* 43:2725–2745. doi:[10.1007/s00382-014-2089-5](https://doi.org/10.1007/s00382-014-2089-5)
- Huffman GJ, Adler RF, Morrissey MM, Bolvin DT, Curtis S, Joyce R, McGavock B, Susskind J (2001) Global precipitation at one-degree daily resolution from multisatellite observations. *J Hydrometeorol* 2:36–50. doi:[10.1175/1525-7541\(2001\)002<0036:GPAODD>2.0.CO;2](https://doi.org/10.1175/1525-7541(2001)002<0036:GPAODD>2.0.CO;2)
- Izumo T, Montégut CB, Luo JJ, Behera SK, Masson S, Yamagata T (2008) The role of the western Arabian Sea upwelling in Indian monsoon rainfall variability. *J Climate* 21:5603–5623. doi:[10.1175/2008JCLI2158.1](https://doi.org/10.1175/2008JCLI2158.1)
- Krishnan R, Ramesh KV, Samala BK, Meyers G, Slingo JM, Fennessy MJ (2006) Indian Ocean—monsoon coupled interactions and impending monsoon droughts. *Geophys Res Lett* 33:L08711. doi:[10.1029/2006GL02581](https://doi.org/10.1029/2006GL02581)
- Lee JY, Wang B, Kang IS, Shukla J, Kumar A, Kug JS, Schemm JKE, Luo JJ, Yamagata T, Fu X, Alves O, Stern B, Rosati T, Park-Show CK (2010) How are seasonal prediction skills related to models' performance on mean state and annual cycle? *Clim Dyn* 35(2):267–283. doi:[10.1007/s00382-010-0857-4](https://doi.org/10.1007/s00382-010-0857-4)
- Lee Drbohlav H, Krishnamurthy V (2010) Spatial structure, forecast errors, and predictability of the South Asian monsoon in CFS monthly retrospective forecasts. *J Clim* 23:4750–4769. doi:[10.1175/2010JCLI2356.1](https://doi.org/10.1175/2010JCLI2356.1)
- Levine RC, Turner AG (2012) Dependence of Indian monsoon rainfall on moisture fluxes across the Arabian Sea and the impact of coupled model sea surface temperature biases. *Clim Dyn* 38(11–12):2167–2190
- Levine RC, Turner AG, Marathayil D, Martin GM (2013) The role of northern Arabian Sea surface temperature biases in CMIP5 model simulations and future projections of Indian summer monsoon rainfall. *Clim Dyn* 41:155–172. doi:[10.1007/s00382-012-1656-x](https://doi.org/10.1007/s00382-012-1656-x)
- Masumoto Y, Meyers G (1998) Forced Rossby waves in the southern tropical Indian Ocean. *J Geophys Res* 103:27589–27602
- Meehl GA, Arblaster JM, Caron JM, Annamalai H, Jochum M, Chakraborty A, Murtugudde R (2012) Monsoon regimes and processes in CCSM4. Part I: the Asian–Australian monsoon. *J Clim* 25:2583–2608. doi:[10.1175/JCLI-D-11-00184.1](https://doi.org/10.1175/JCLI-D-11-00184.1)
- Murtugudde R, Busalacchi AJ (1999) Interannual variability of the dynamics and thermodynamics of the tropical Indian Ocean. *J Clim* 12:2300–2326. doi:[10.1175/1520-0442\(1999\)012<2300:IVO TDA>2.0.CO;2](https://doi.org/10.1175/1520-0442(1999)012<2300:IVO TDA>2.0.CO;2)
- Murtugudde R, Goswami B, Busalacchi A (1998) Air–sea interaction in the Southern Tropical Indian Ocean and its relation to interannual variability of the monsoon over Indian. In: International conference on monsoon and hydrologic cycle, Korean Meteorological Society, pp184–188
- Narapusetty B, DelSole T, Tippett MK (2009) Optimal estimation of the climatological mean. *J Clim* 22:4845–4859. doi:[10.1175/2009JCLI2944.1](https://doi.org/10.1175/2009JCLI2944.1)
- Narapusetty B, Stan C, Kumar A (2014) Bias correction methods for decadal sea-surface temperature forecasts. *Tellus A*. doi:[10.3402/tellusa.v66.23681](https://doi.org/10.3402/tellusa.v66.23681) (ISSN 1600-0870)
- Neale R, Slingo J (2003) The maritime continent and its role in the global climate: a GCM study. *J Clim* 16:834–848. doi:[10.1175/1520-0442\(2003\)016<0834:TMCAIR>2.0.CO;2](https://doi.org/10.1175/1520-0442(2003)016<0834:TMCAIR>2.0.CO;2)
- Pottapinjara V, Girishkumar MS, Ravichandran M, Murtugudde R (2014) Influence of the Atlantic zonal mode on monsoon depressions in the Bay of Bengal during boreal summer. *J Geophys Res Atmos* 19(11):6456–6469. doi:[10.1002/2014JD021494](https://doi.org/10.1002/2014JD021494)
- Rajeevan M (2001) Prediction of Indian summer monsoon: Status, problems and prospects. *Curr Sci* 81:1451–1457 (ISSN 0011-3891)
- Reynolds RW, Rayner NA, Smith TM, Stokes DC, Wang W (2002) An improved in situ and satellite SST analysis for climate. *J Clim* 15:1609–1625. doi:[10.1175/1520-0442\(2002\)015<1609:AIIASAS>2.0.CO;2](https://doi.org/10.1175/1520-0442(2002)015<1609:AIIASAS>2.0.CO;2)
- Saha S, Moorthi S, Pan H-L, Wu X, Wang J, Nadiga S, Tripp P, Kistler R, Woollen J, Behringer D, Liu H, Stokes D, Grumbine R, Gayno G, Wang J, Hou Y-T, Chuang H-Y, Juang HMH, Sela J, Iredell M, Treadon R, Kleist D, Delst PV, Keyser D, Derber J, Ek M, Meng J, Wei H, Yang R, Lord S, Van Den Dool H, Kumar A, Wang W, Long C, Chelliah M, Xue Y, Huang B, Schemm JK, Ebisuzaki W, Lin R, Xie P, Chen M, Zhou S, Higgins W, Zou C-Z, Liu Q, Chen Y, Han Y, Cucurull L, Reynolds RW, Rutledge G, Goldberg M (2010) The NCEP climate forecast system reanalysis. *Bull Am Meteorol Soc* 91:1015–1057. doi:[10.1175/2010BAMS3001.1](https://doi.org/10.1175/2010BAMS3001.1)
- Saha S, Moorthi S, Wu X, Wang J, Nadiga S, Tripp P, Behringer D, Hou Y, Chuang H, Iredell M, Ek M, Meng J, Rongqian Yang



- R, Mendez MP, van den Dool H, Zhang Q, Wang W, Chen M, Becker E (2014) The NCEP climate forecast system version 2. *J Clim* 27:2185–2208. doi:[10.1175/JCLI-D-12-00823.1](https://doi.org/10.1175/JCLI-D-12-00823.1)
- Sahana AS, Ghosh S, Ganguly A, Murtugudde R (2015) Shift in Indian summer monsoon onset during 1976/1977. *Environ Res Lett* 10:054006. doi:[10.1088/1748-9326/10/5/054006](https://doi.org/10.1088/1748-9326/10/5/054006)
- Sayantani O, Gnanaseelan C, Chowdary JS (2014) The role of Arabian Sea in the evolution of Indian Ocean Dipole. *Int J Clim* 34(6):1845–1859
- Shukla J (1975) Effect of Arabian sea-surface temperature anomaly on Indian summer monsoon: a numerical experiment with the GFDL model. *J Atmos Sci* 32:503–511
- Sikka DR, Gadgil S (1980) On the maximum cloud zone and the ITCZ over Indian, longitudes during the southwest monsoon. *Mon Weather Rev* 108:1840–1853. doi:[10.1175/15200493\(1980\)108<1840:OTMCZA>2.0.CO;2](https://doi.org/10.1175/15200493(1980)108<1840:OTMCZA>2.0.CO;2)
- Slingo JM, Annamalai H (2000) The El Niño of the century and the response of the Indian summer monsoon. *Mon Weather Rev* 128:1778–1797. doi:[10.1175/1520-0493\(2000\)128<1778:TENO OT>2.0.CO;2](https://doi.org/10.1175/1520-0493(2000)128<1778:TENO OT>2.0.CO;2)
- Vecchi GA, Harrison DE (2004) Interannual Indian rainfall variability and Indian Ocean sea surface temperature anomalies. *Earth's climate: the ocean atmosphere interaction*. *Geophys Monogr Am Geophys Union* 147:247–259
- Vecchi GA, Xie SP, Fischer AS (2004) Ocean–atmosphere covariability in the Western Arabian Sea. *J Clim* 17:1213–1224. doi:[10.1175/1520-0442\(2004\)017<1213:OCITWA>2.0.CO;2](https://doi.org/10.1175/1520-0442(2004)017<1213:OCITWA>2.0.CO;2)
- Xie P, Arkin PA (1997) Global precipitation: a 17-year monthly analysis based on gauge observations, satellite estimates, and numerical model outputs. *Bull Am Meteorol Soc* 78:2539–2558. doi:[10.1175/1520-0477\(1997\)078<2539:GPAYMA>2.0.CO;2](https://doi.org/10.1175/1520-0477(1997)078<2539:GPAYMA>2.0.CO;2)
- Yang GY, Slingo J (2001) The diurnal cycle in the tropics. *Mon Weather Rev* 129(4):784–801. doi:[10.1175/15200493\(2001\)129<0784:TDCITT>2.0.CO;2](https://doi.org/10.1175/15200493(2001)129<0784:TDCITT>2.0.CO;2)
- Yatagai A, Kamiguchi K, Arakawa O, Hamada A, Yasutomi N, Kito A (2012) APHRODITE: constructing a long-term daily gridded precipitation dataset for Asia based on a dense network of rain gauges. *Bull Am Meteorol Soc* 93:1401–1415. doi:[10.1175/BAMS-D-11-00122.1](https://doi.org/10.1175/BAMS-D-11-00122.1)
- Zhou L, Murtugudde R (2010) Influences of Madden–Julian oscillations on the eastern Indian Ocean and the maritime continent. *Dyn Atmos Oceans* 2:257–274. doi:[10.1016/j.dynatmoce.2009.12.003](https://doi.org/10.1016/j.dynatmoce.2009.12.003)
- Zhou L, Murtugudde R (2014) Impact of northward propagating intraseasonal variability on the onset of Indian summer monsoon. *J Clim* 27:126–139. doi:[10.1175/JCLI-D-13-00214.1](https://doi.org/10.1175/JCLI-D-13-00214.1)
- Zhou L, Murtugudde R, Jochum M (2008a) Dynamics of the intraseasonal oscillations in the Indian Ocean South Equatorial Current. *J Phys Oceanogr* 38:121–132. doi:[10.1175/2007JPO3730.1](https://doi.org/10.1175/2007JPO3730.1)
- Zhou L, Murtugudde R, Jochum M (2008b) Seasonal influence of Indonesian through flow in the southwestern Indian Ocean. *J Phys Oceanogr* 38:1529–1541